DOI: 10.6060/mhc256957m

# Enhanced Synthesis and Photodynamic Anticancer and Antimicrobial Activities of Tetra(pentafluorophenyl)bacteriochlorin

Kaisano G. Tauyakhale,[a] Mahlatse M. Ledwaba,[a] Earl Prinsloo,[b] John Mack,[a@] and Tebello Nyokong[a]

[a]*Tebello Nyokong Institute of Nanotechnology Innovation, Rhodes University, Makhanda 6140, South Africa*
[b]*Biotechnology Innovation, Centre, Rhodes University, Makhanda 6140, South Africa*
[@]*Corresponding author E-mail: j.mack@ru.ac.za*

*The potential utility of meso-pentafluorobacteriochlorin (**PentaBChl**), a readily synthesized porphyrin analogue that absorbs significantly in the near-infrared region, for photodynamic therapy (PDT) and photodynamic antimicrobial chemotherapy (PACT) was investigated. Identifying suitable dyes that absorb significantly in the 700−800 nm region is particularly important from an African perspective, since melanin significantly limits the penetration of laser light into human tissue in the 600−700 nm region, where first- and second-generation photosensitizer dyes usually absorb. A modified solvent-free synthetic approach was developed to prepare **PentaBChl** from the commercially available meso-pentafluoroporphyrin (**PentaP**) parent dye in high yield. The in vitro PDT activities of **PentaP** and **PentaBChl** were compared against MCF-7 breast cancer cells through 30 min of irradiation with M595L3 (2.7 J/cm$^2$) and M730L4 (1.7 J/cm$^2$) Thorlabs light-emitting diodes (LEDs). An $IC_{50}$ value of 7.6 μM was obtained for **PentaBChl**, comparable to values reported previously for tetraarylchlorins, despite a significantly lower singlet oxygen quantum yield of 0.21. In vitro PACT activity studies were conducted against S. aureus and E. coli, as typical examples of Gram-(+) and Gram-(−) bacterial strains, through 60 min of irradiation with M595L3 (5.4 J/cm$^2$) and M730L4 (3.4 J/cm$^2$) Thorlabs LEDs. $Log_{10}$ reduction values of 3.49 and 5.89 were observed for **PentaBChl** against S. aureus and E. coli, respectively, after incubation at 80 μM. These results demonstrate that the PDT and PACT activity properties of tetraarylbacteriochlorins merit further in-depth investigation.*

**Keywords:** Bacteriochlorins, porphyrins, singlet oxygen, photodynamic therapy, photodynamic antimicrobial chemotherapy, photosensitizer dyes.

# Оптимизированный синтез и фотодинамическая противораковая и противомикробная активность тетра(пентафторфенил)бактериохлорина

К. Г. Тауяхале,[a] М. М. Ледваба,[a] Э. Принслу,[b] Д. Мак,[a@] Т. Ниоконг[a]

[a]*Институт нанотехнологических инноваций Тебелло Ниоконг, Университет Родса, Маханда 6140, Южная Африка*
[b]*Центр биотехнологических инноваций, Университет Родса, Маханда 6140, Южная Африка*
[@]*E-mail: j.mack@ru.ac.za*

*Исследованы перспективы использования мезо-пентафторбактериохлорина (**PentaBChl**), легко синтезируемого аналога порфирина, значительно поглощающего излучение в ближнем инфракрасном диапазоне, в фотодинамической терапии (ФДТ) и фотодинамической антимикробной химиотерапии (ФАХТ). Выявление подходящих красителей, значительно поглощающих излучение в диапазоне 700–800 нм, особенно важно для африканских стран, поскольку меланин значительно ограничивает проникновение лазерного света в ткани человека в диапазоне 600–700 нм, где обычно поглощают фотосенсибилизирующие красители первого и второго поколений. Был разработан подход для получения **PentaBChl** без использования растворителя из коммерчески доступного исходного красителя мезо-пентафторпорфирина (**PentaP**) с высоким выходом. Активность фотодинамической терапии (ФДТ) **PentaP** и **PentaBChl** in vitro сравнивали с клетками рака мо-*

  

*лочной железы MCF-7 при 30-минутном облучении светодиодами Thorlabs M595L3 (2,7 Дж/см²) и M730L4 (1,7 Дж/см²). Для **PentaBChl** было получено значение $IC_{50}$=7,6 мкМ, сопоставимое со значениями, ранее сообщенными для тетраарилхлоринов, несмотря на значительно более низкий квантовый выход синглетного кислорода (0,21). Исследования активности фотоакустической терапии in vitro проводили относительно S. aureus и E. coli, типичных примеров грамположительных и грамотрицательных бактериальных штаммов, при 60-минутном облучении светодиодами Thorlabs M595L3 (5,4 Дж/см²) и M730L4 (3,4 Дж/см²). Значения снижения концентрации **PentaBChl** по логарифмической шкале (lg) составили 3,49 и 5,89 для S. aureus и E. coli, соответственно, после инкубации при концентрации 80 мкМ. Эти результаты показывают, что свойства тетраарилбактериохлоринов в отношении фотодинамической терапии (ФДТ) и фотоакустической терапии (ФАКТ) заслуживают дальнейшего углубленного исследования.*

**Ключевые слова:** Бактериохлорины, порфирины, синглетный кислород, фотодинамическая терапия, фотодинамическая антимикробная химиотерапия, фотосенсибилизаторы.

## Introduction

Cancer is reported to be the leading cause of death worldwide (1 in 6 deaths are due to cancer). Moreover, it is reported that cancer kills more people than tuberculosis, malaria, and AIDS combined every year.[1,2] Chemotherapy has been utilized as a mode of rehabilitation for complete remission, being used in conjunction with surgery or to improve the state of well-being of patients until their point of death.[3,4] However, it is well known for its adverse side effects, such as loss of hair, altered gastric metabolism, vomiting and nausea, dehydration, weight loss, and loss of appetite.[5] For this reason, photodynamic therapy (PDT) has been developed as an alternative.[6] During PDT, a photosensitizer (PS) dye and light of a specific wavelength produce cytotoxic singlet oxygen species, which induce cell death. A PS dye is photoexcited by light of a specific wavelength and undergoes intersystem crossing to the triplet manifold, which reacts with oxygen molecules to form $^1O_2$, a Type II energy transfer reaction, or to form other reactive oxygen species (ROS) via a Type I electron transfer mechanism.[6,7]

In this study, a bacteriochlorin (BChl) was chosen as the main target PS dye because, unlike their structural analogues, porphyrins and chlorins, BChls absorb light in the near-infrared region (NIR) well within the therapeutic window.[8] This enhances tissue penetration when excited by an appropriate light source.[9,10] NIR photons can give direct access to biological targets because they are the most invasive and least harmful to human tissues. The phototherapeutic window lies between 620 and 850 nm, where light can penetrate tissue to depths of 1−3 cm.[10,11] BChls have ideal properties for use as PS dyes, including ease of synthesis, solubility in a variety of solvents, high singlet oxygen quantum yields, long triplet state lifetimes and most importantly nontoxic and rapid clearance out of the body after therapy unlike most Food & Drug Administration (FDA) approved PSs, such as Photofrin, Levulan, Metvix and Photochlor, which are reported to take a long time to be expelled by the body, leading to long-term skin photosensitivity.[12-16] Lastly, most commercial PS dyes are activated by more blue-shifted light in the 600–700 nm region, thereby making deep tissue penetration impossible to achieve. Identifying suitable dyes that absorb significantly in the 700−800 nm region is particularly important from an African perspective, since melanin significantly limits the penetration of laser light into human tissue in the 600−700 nm region, where first- and second-generation photosensitizer dyes usually absorb.[17] The PS dyes selected for study in this context are free-base tetra(pentafluorophenyl)-porphyrin (**PentaP**) and bacteriochlorin (**PentaBChl**), since promising PDT activity properties have been reported recently for **PentaBChl** in polyethylene glycol nanogels by Zhang and coworkers.[18] Electron-withdrawing pentafluorophenyl groups were introduced at the *meso*-positions to enhance dye stability.[19,20] The *in vitro* PDT activities of **PentaP** and **PentaBChl** were compared against Michigan Cancer Foundation-7 (MCF-7) breast cancer cells in a similar manner to recent studies at the Institute for Nanotechnology Innovation (INI) at Rhodes University on tetraarylchlorins,[15] while the *in vitro* photodynamic antimicrobial chemotherapy (PACT) activities of these dyes were compared against *S. aureus* and *E. coli* as typical examples of Gram-(+) and Gram-(−) bacterial strains. PACT has emerged as an alternative approach for treating bacteria that have developed antibacterial resistance.[21] Naturally formed bacteriochlorins have recently been reported to exhibit promising properties in this regard.[22]

## Experimental

### *Materials*

Pentafluorobenzaldehyde, propionic acid, nitric acid, pyrrole, sodium hydroxide, pyridine, potassium carbonate, *p*-toluenesulfonylhydrazide, dimethysulfoxide (DMSO), hexane, zinc tetraphenylporphyrin (ZnTPP), 9,10-dimethylanthracene (DMA), MTT (3-[4,5-dimethylthiazol-2-yl]-2,5-diphenyl tetrazolium bromide), and $CDCl_3$ were obtained from Sigma-Aldrich. Chloroform was purchased from Minema. Type II water for the *in vitro* studies was sourced from an Elga Purelab Chorus 2 (RO/DI) system. Dulbecco's modified Eagle's medium (DMEM) and phosphate-buffered saline (DPBS) were supplied by Lonza®. The MCF-7 cells used for *in vitro* PDT activity studies were obtained from Cellonex®, while heat-inactivated fetal calf serum (FCS), 100 µg/mL streptomycin-amphotericin B, penicillin streptomycin-amphotericin B mix, and 100 units/mL penicillin at tissue culture grade were obtained from Biowest®. *In vitro* PACT studies were carried out with *S. aureus* and *E. coli* (ATCC® 25923™ and 25922™) obtained from Davies Diagnostics. Reagents were used as supplied, except for pyrrole, which was distilled before use.

## *Equipment*

A Shimadzu UV-2550 spectrometer was used to measure ground state electronic absorption spectra at room temperature in a 1 cm pathlength quartz cuvette over a wavelength range of 300−800 nm. A Varian Eclipse spectrofluorimeter was used during the fluorescence quantum yield ($\Phi_F$) studies by using the comparative method[23] in DMSO, with ZnTPP ($\Phi_F$ = 0.039[24]) used as the standard. A Bruker 85 MHz benchtop NMR instrument was used to obtain the $^1$H NMR data. The spectrum was measured at ambient temperature using $CDCl_3$. Mass spectral data were obtained using a Bruker Auto-FLEX III Smartbeam MALDI-TOF mass spectrometer in positive ion mode with α-cyano-4-hydroxycinnamic acid as the matrix. An Ekspla NT 342B-20-AW laser with an Nd:YAG that pumps a 420−2300 nm optical 30 parametric oscillator (OPO) (355 nm, 2.0 mJ/7 ns, 20 Hz) was used to provide monochromatic light at a crossover wavelength for singlet oxygen quantum yield ($\Phi_\Delta$) measurements in DMSO for the standard (ZnTPP; $\Phi_\Delta$ = 0.53[25]) and sample with DMA as the singlet oxygen scavenger. The Eskpla NT342B-20-AW laser also provided the pump beam for an Edinburgh Instruments LP980 transient absorption spectrometer fitted with a PMT-LP (Hamamatsu R928P). This instrument was used to determine the triplet state lifetime ($\tau_T$) values. The bioillumination kit of a Modulight® Medical Laser 7710-680 system was fitted with Thorlabs M595L3 and M730L4 light-emitting diodes (LEDs) during the PDT and PACT studies, with maximum outputs at 595 and 730 nm to match the lower energy Q band wavelengths for **PentaP** and **PentaBChl**, respectively. The outputs from the LEDs were measured with a Coherent FieldmaxII TOP energy/power meter fitted with a Coherent Powermax PM10 sensor. A Scan® 500 automatic colour colony counter was utilized for the PACT activity studies, while a Synergy 2 multi-mode microplate reader (BioTek®) was used for the PDT activity studies. A fluorescence LED inverted microscope was used to observe the morphology of the MCF-7 breast cancer cells before and after the PDT activity studies under phase contrast (Zeiss-AxioVert). Porvair 25 cm$^2$ vented flasks were utilized during MCF-7 cell culture preparations.

## *Synthesis*

**PentaP** is commercially available, but in the context of this study, it was prepared from pentafluorobenzaldehyde and pyrrole according to the Adler-Longo method,[26] while a modified solvent-free method was developed to prepare **PentaBChl** (Scheme 1). Firstly, a 3:1 mixture of *p*-toluenesulfonylhydrazide/**PentaP** (50 mg) was ground for 30 min. Then, the green slurry formed through mixing was heated with constant stirring at 80 °C for 15 min. The product was purified by silica column chromatography with chloroform as the eluent. 5,10,15,20-Tetrakis(pentafluorophenyl)-7H,8H,17H,18H-porphyrin (**PentaBChl**) – black crystals (21 mg, 42% yield) were obtained. $^1$H NMR (80 MHz, $CDCl_3$) δ ppm: 2.34 (s, 8H), 7.46 (s, 2H), 7.16 (s, 2H), 2.34 (s, 8H), −2.74 (s, 2H). MALDI-TOF *m/z*: 978.09 obtained, 978.40 calculated.

## *Antimicrobial studies*

For the antibacterial activity investigations, multidrug-resistant Gram-(+) *Staphylococcus aureus* (*S. aureus*) and Gram-(−) *Escherichia coli* (*E. coli*) were utilized. In a similar manner to the PDT assay below, these antimicrobial investigations were carried out using 1% DMSO due to issues with dye solubilization. Additionally, for dependability, validity, and repeatability, they were completed in independent triplicates. Added to this, toxicity under both light and dark conditions was also assessed to evaluate whether these compounds would be ideal photosensitizers that are only active when exposed to radiation. The cultured bacterial colonies were inoculated into nutrient broth and were agitated for 24 h at 37 °C in a rotating shaker. Afterwards, the culture aliquots were transplanted to 5 mL of fresh broth and cultured until they reached a mid-logarithmic phase (optical density (OD) at 620 nm ≈ 0.6). To determine the log reduction values in Colony Forming Units (CFU)/mL, the OD of the bacterial culture was measured using a Ledetect 96 from Labxim Products. Using DPBS, the bacterial broth was centrifuged for 10 min at 4000 rpm to wash it. The collected bacteria were resuspended with a dilution factor of $10^{-6}$ in 100 mL DPBS, which served as the bacterial stock solution. Different concentrations of fresh bacterial stock solutions were prepared at 0, 20, 40, 60, 80, and 100 μM of the photosensitizer dye.

Following a 30 min incubation period to allow the compounds to internalize, 3 mL of the bacteria-PS stock solution, which had a volume of 6 mL, was pipetted onto each of two distinct 24-well plates. A Modulight 710-680 medical laser fitted with a Thorlabs LED of the appropriate wavelength was used to irradiate one of the 24-well plates for 60 min, while the other was left in the dark. The LEDs used were an M595L3 (5.4 J/cm$^2$) for **PentaP** and an M730L4 (3.4 J/cm$^2$) for the **PentaBChl**. Following this, 100 μL of each sample concentration was pipetted onto nutrient agar-coated Petri dishes. The plates were left in the dark for 24 h at 37 °C. To calculate the CFU/mL values for the colonies that formed, a Scan 500 Automatic Colony Counter from Healthcare Technologies was utilized. To select an appropriate compound concentration that demonstrated optimal antimicrobial activity characteristics for the subsequent time-dependency investigations, a concentration-dependence analysis was initially carried out.

The bacterial-compound solution was prepared for time-dependent investigations and introduced into a 24-well plate using the same process described above. 100 μL of the sample was pipetted onto nutrient agar-coated Petri dishes after each 10 min of radiation. The samples were then incubated for 24 h, and CFU/mL values were determined using the protocol described above. Survival fractions were determined by contrasting the control (Petri dishes containing only bacteria) with those treated with the PS dye. The investigation was conducted in triplicate to facilitate the calculation of standard deviations.

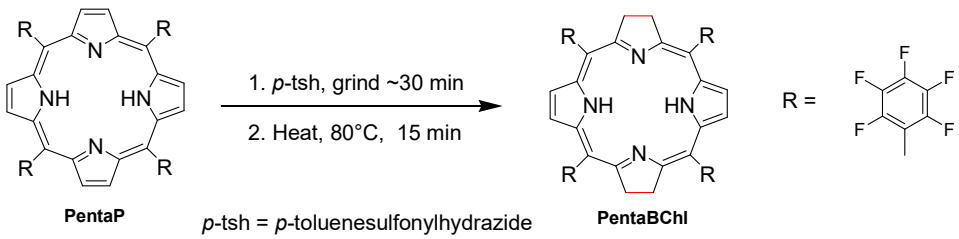


**Scheme 1.** The solvent-free synthesis of **PentaBChl** from **PentaP**. Red bonds highlight the reduction of peripheral bonds in the BChl ligand.

### *Anticancer studies*

The cells used for the PDT activity studies were MCF-7 breast cancer cells. Since the dyes had limited solubility in aqueous solution, these preliminary proof-of-principle anticancer investigations were carried out using 1% DMSO. This was necessary due to issues with dye solubilization. Additionally, to ensure dependability, validity, and repeatability, the studies were conducted using independent triplicates. A substance's ability to inhibit a particular biological or biochemical process is measured by its half-maximal inhibitory concentration ($IC_{50}$), which also indicates how much of a pharmacological agent is needed to reduce biological activity by half. In order to calculate this value, the cell viability was assessed using the MTT assay[27] and Equation 1:

$$\% \, Cell \, viability = \frac{OD_{\lambda} Treated \, cells}{OD_{\lambda} Control \, cells} \times 100 \quad (1)$$

The malignant cells were grown in separate T75 $cm^2$ cell culture flasks using DMEM containing 10% FCS and 0.01% antibiotics (penicillin and streptomycin-amphotericin B). The cells were grown to 100% confluence by incubating at 37°C under 5% $CO_2$. The cells were seeded in DMEM medium in 96-well plates and were incubated for 24 h under 5% $CO_2$. Following this, the cells were once more incubated in the dark for 24 h, this time in a fresh DMEM mixture with varying quantities of **PentaP** and **PentaBChl** (0, 20, 40, 60, 80, and 100 μM). A separate set of 96-well plates served as controls; these plates were loaded with new DMEM without the synthesized compounds. The medium containing the dyes was removed once the specified incubation period had elapsed, and fresh DMEM free of phenol red was introduced. The cells were then exposed to light for 30 min using a Thorlabs LED fitted onto the casing of a Modulight 7710-680 medical laser with a wavelength suitable for the compounds under study. The Thorlabs LEDs used were an M595L3 (2.7 J/$cm^2$) for **PentaP** and an M730L4 (1.7 J/$cm^2$) for the **PentaBChl**. The cells were cultured for a further 24 h after the clear DMEM medium was discarded and replaced with fresh DMEM containing 10% FCS. An extra batch of cells treated with the compounds was prepared; no irradiation was applied during the dark toxicity studies. Following a 24 h incubation period, the media was removed, DMEM-10% FCS was added, and the cells were incubated for a further 24 h. Following this, the media was properly disposed of, and each well was filled with 25 μL of MTT (5 mg/mL) diluted in PBS (phosphate-buffered saline). The cells were then incubated for 3 h in the absence of light. A Molecular Devices Spectra Max M5 plate reader was used to measure the formazan absorbance at 545 nm. The percentage ratio of treated cells' absorbance to that of the untreated control provides the cytotoxicity measurement. GraphPad Prism was used to determine the $IC_{50}$ for **PentaBChl** via nonlinear regression analysis.

### *Theoretical calculations*

Geometry optimizations were carried out for **PentaP** and **PentaBChl** at the B3LYP/SDD level of theory by using the Gaussian 09 software package[28] on the Lengau cluster of the Centre for High Performance Computing in Cape Town. The default SDD basis sets were selected. Time-dependent density functional theory (TD-DFT) calculations were carried out at the CAM-B3LYP/SDD level of theory to analyze further the molecular implications of the structural modifications of the porphyrinoids selected for this study. The CAM-B3LYP functional was selected since it contains a long-range correction.[29] **PentaP** and **PentaBChl** were studied to determine the effect of the reduction of the ligand along the *y*-axis on the frontier π-MOs that determine the optical properties.

## Results and Discussion

### *Synthesis and characterization*

The preparation of **PentaBChl** was found to be very challenging using previously reported methods,[30,31] as the reduction from chlorin to BChl does not readily proceed to completion, necessitating challenging chromatography. Although it is technically feasible, chromatographic purification of bacteriochlorins is extremely challenging because the reaction usually produces a mixture of porphyrin, chlorin, and bacteriochlorin derivatives with extremely similar molecular weights and structures. For this reason, a solvent-free method[18] was utilized, with modifications identified by trial and error, to obtain optimal yields of the **PentaBChl** target dye. Firstly, an initially 3:1 *p*-toluenesulfonylhydrazide/porphyrin (0.50 g) mixture was ground for 30 min with a mortar and pestle, with monitoring by UV-visible absorption spectroscopy in methanol solution at 10 min intervals to check for the disappearance of the chlorin band maximum at *ca.* 650 nm and concomitant increase in the intensity of the BChl band at *ca.* 740 nm as the color of the mixture steadily changes from off-white to green. Once the lowest-energy band of **PentaBChl** becomes more intense than that of the chlorin intermediate, the green slurry obtained from the grinding step was heated at 80°C for 15 min with constant stirring, rather than at reflux, to obtain the stable BChl target product with no obvious porphyrin and chlorin UV-visible absorption bands. Silica gel chromatography was still conducted with chloroform as the eluent with the goal of achieving the maximum possible level of purity for the **PentaBChl** product. There is no need to conduct these steps under an inert atmosphere. The **PentaBChl** product was purified by silica gel column chromatography with chloroform as the eluent. The anticipated peak at −2.74 ppm for the two inner NH protons was observed, along with the eight-proton peak for the reduced pyrrolic bonds *ca.* 2.34 ppm, and peaks arising from the four β-pyrrolic protons in the aromatic region. The calculated molecular mass for **PentaBChl** is 978.09 amu, while the MALDI-TOF MS peak was observed at 978.40 *m/z*.

### *UV-visible absorption spectroscopy and molecular modelling*

There is a marked red shift of the lower energy Q band of **PentaBChl** to 754 nm in DMSO relative to 654 nm for **PentaP**, while the higher energy Q band blue shifts to 508 nm relative to 584 nm for **PentaP** (Figure 1 and Table 1). In a similar manner, there is a blue shift and splitting of the B bands of **PentaBChl** at 375 and 345 nm relative to that of **PentaP** at 406 nm. Both dyes were observed to aggregate significantly in DMSO solution. Conceptual frameworks such as Gouterman's 4-orbital model and Michl's perimeter model can be used to identify trends in the energies of the four frontier orbital MOs that are derived from the HOMO and LUMO of a parent $C_{16}H_{16}^{2-}$ parent perimeter with a $M_L$ = 0, ±1, ±2, ±3, ±4, ±5, ±6, ±7, 8 sequence in ascending energy terms. According to the Gouterman four-orbital model,[32] the four frontier molecular orbitals that determine the UV-visible spectra of porphyrins under $D_{4h}$ symmetry are a dou-

bly degenerate LUMO (**a** and **s** in terms of Michl's perimeter model[33]) and a pair of accidentally degenerate HOMO and HOMO−1 (**-a** and **-s**) that are derived from the HOMO of the parent $C_{16}H_{16}^{2-}$ parent hydrocarbon perimeter. The energy splitting of the **a** and **s** MOs is described as a change in the ΔHOMO value in the context of Michl's perimeter model,[33] while the energy splitting of the **-a** and **-s** MOs is described by the change in the ΔLUMO value. Changes in the electronic absorption bands of porphyrinoids can be explained on the basis of modifications to the relative energies of the four frontier orbitals and the ΔHOMO and ΔLUMO values when structural modifications are introduced. The percentage contributions of the one-electron transitions between the **a**, **s**, **-a** and **-s** MOs for the Q and B bands of **PentaP** are *ca.* 50% (Table 2), as is normally anticipated for the porphyrin ligand.[34] The electron dipole transition moments cancel in the case of the Q band, resulting in nearly fully forbidden Q bands with $\Delta M_L = \pm 9$ properties, while they add together in the case of the B transitions, resulting in fully allowed B bands with $\Delta M_L = \pm 1$ properties.

When the **PentaP** ligand is reduced to form **PentaBChl**, the one-electron transition percentages are significantly modified (Table 2) due to the significant ΔHOMO and ΔLUMO values introduced when the ligand periphery is doubly reduced along the *y*-axis. This results in an intensification of the lowest energy Q band since the electron dipole transition moments no longer cancel, enhancing the suitability of the dyes for use in PDT. The HOMO−LUMO gap narrows significantly due to a relative destabilization of the **a** MO, which has large MO coefficients at the ligand periphery (Figure 2), resulting in a large red shift of the Q bands. A significant discrepancy is observed between the calculated and experimentally observed band maxima because TD-DFT calculations systematically overestimate the energies of the Q and B bands of porphyrins and their analogues.[34]

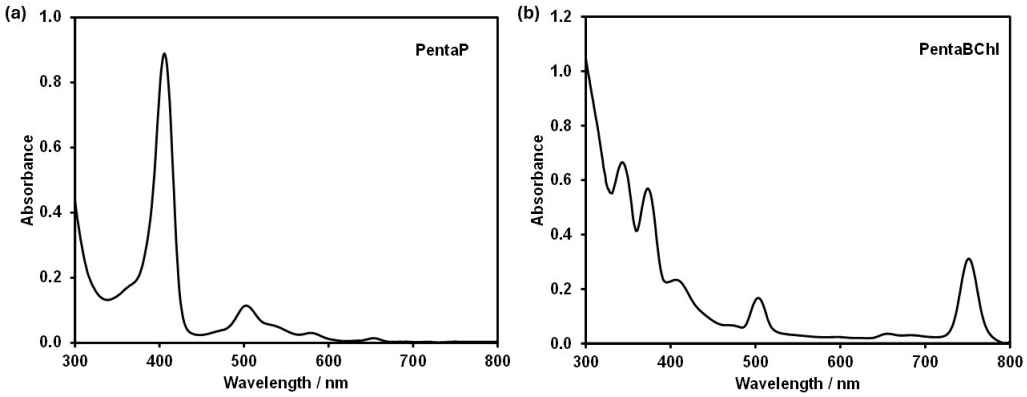


**Figure 1.** (a) UV-visible absorption spectra of (a) **PentaP** and (b) **PentaBChl** in DMSO.

**Table 1.** The photophysicochemical properties of **PentaP** and **PentaBChl** in DMSO.

| | Abs ($\lambda_{max}$) | Emission ($\lambda_{max}$) | $\Phi_F$ | $\Phi_\Delta$ | $\tau_T$ (μs) | Photostability |
|---|---|---|---|---|---|---|
| **PentaP** | 406, 503, 584, 654 | 703 | 0.06 | 0.37 | 39 | 98% |
| **PentaBChl** | 345, 375, 410, 508, 754 | -- | -- | 0.21 | 74 | 98% |

**Table 2.** Calculated and experimental electronic excitation wavelengths of **PentaP** and **PentaBChl**, and their respective calculated wavenumbers and wavefunctions, were calculated at the CAM-B3LY/SDD level of theory.

| #[a] | Band[b] | $\nu \cdot 10^3$ ($cm^{-1}$)[c] | $\lambda_{calc}$(nm)[d] | $\lambda_{exp}$(nm)[e] | f[f] | Wavefunction =[g] |
|---|---|---|---|---|---|---|
| | | | **PentaP** | | | |
| 1 | Q | 17.0 | 589 | 654 | 0.00 | 55% **s** → **-s**; 45% **a** → **-a**; … |
| 2 | Q | 19.0 | 526 | 584 | 0.00 | 51% **s** → **-a**; 49% **a** → **-s**; … |
| 3 | B | 26.8 | 373 | 406 | 1.00 | 48% **a** → **-a**; 31% **s** → **-s**; … |
| 4 | B | 28.2 | 355 | | 1.64 | 51% **a** → **-s**; 47% **s** → **-a**; … |
| | | | **PentaBChl** | | | |
| 1 | Q | 14.8 | 678 | 753 | 0.33 | 90% **a** → **-s**; … |
| 2 | Q | 19.9 | 502 | 508 | 0.14 | 74% **s** → **-s**; 25% **a** → **-a**; … |
| 3 | B | 30.2 | 332 | 375 | 1.49 | 76% **a** → **-a**; 27% **s** → L+3; … |
| 4 | B | 32.5 | 308 | 345 | 1.09 | 63% **s** → **-a**; 27% **a** → **-s**; … |

[a]Excited state number of TD-DFT calculations. [b]Porphyrin band assignments. [c]Wavenumbers obtained from TD-DFT calculations. [d]Calculated wavelengths in nanometers. [e]Experimental wavelengths in nanometers. [f]Calculated oscillator strengths. [g]Using eigenvectors predicted by TD-DFT, the wavefunctions that define the MOs participating in the transition are described. Only contributions greater than 10% are included.

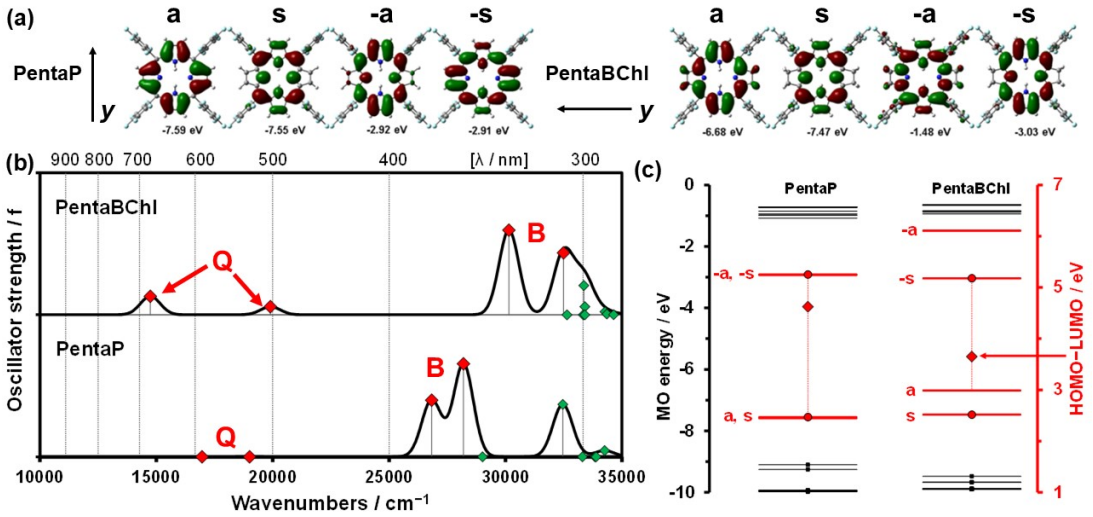


**Figure 2.** (a) The four frontiers π-MOs derived from the HOMO and LUMO of a $C_{16}H_{16}^{2-}$ parent perimeter are referred to as the **a**, **s**, **-a**, and **-s** MOs in the context of Michl's perimeter model.[33] The MO plots are provided at an isosurface of 0.02 a.u. (b) Calculated TD-DFT spectra for **PentaP** and **PentaBChl** at the CAM-B3LYP/SDD level of theory. The simulated spectra were calculated using Chemcraft at a fixed bandwidth of 1500 $cm^{-1}$. Red diamonds are used to highlight the Q and B spectral bands. (c) The MO energies of **PentaP** and **PentaBChl** at the CAM-B3LYP/SDD level of theory. The HOMO and LUMO are highlighted with thick red lines. Black squares denote occupied MOs. Red diamonds highlight HOMO−LUMO gap values plotted against a secondary axis.

## *Photophysical and photochemical properties*

The singlet oxygen quantum yield values for **PentaP** and **PentaBChl** of 0.37 and 0.21 (Table 1), and triplet state lifetime values of 39 and 74 μs, respectively, demonstrate that the dyes are potentially suitable for use during *in vitro* PDT and PACT activity studies. A $\Phi_F$ value of 0.06 was obtained for **PentaP** in DMSO, while no fluorescence was observed for **PentaBChl**. Ideally, PS dyes must be stable under the conditions used for the *in vitro* PDT or PACT activity studies. However, the PS dye tends to undergo self-destructive oxidative photodegradation when generating singlet oxygen during PDT or PACT, resulting in harmful side products that reduce the PDT and PACT activities of the dye. The photostabilities of the dyes were studied in DMSO by monitoring changes in the B band absorption intensities of dyes upon irradiation with M595L3 (2.7 J/$cm^2$) and M730L4 (1.7 J/$cm^2$) Thorlabs LEDs mounted onto the bioillumination kit of a Modulight® Medical Laser 7710-680 system for 30 min in the same manner as for the PDT activity studies. Photostability values of 98% were obtained for both dyes (Table 1), likely due to the electron-withdrawing inductive effects of the *meso*-pentafluorophenyl rings.[18,19]

## *Antimicrobial studies*

*S. aureus* and *E. coli* were selected for study as typical Gram-(+) and -(−) strains, the negative controls in Figures 3 and 4 represent bacteria treated with 5% DMSO in PBS that were not subsequently incubated with the PS dyes studied. A photosensitizer dye concentration of 80 μM was selected for the study, based on preliminary concentration studies. The $Log_{10}$ reduction values are tabulated in Table 3.

**Table 3**. A summary of the $Log_{10}$ reduction values against *S. aureus* and *E coli*.

| PS | Light[a] | Dark |
|---|---|---|
| S. aureus | | |
| PentaP | 2.22 | 0.68 |
| PentaBChl | 3.49 | 0.69 |
| E. coli | | |
| PentaP | 6.39 (@45 min)[a] | 0.87 |
| PentaBChl | 5.89 | 0.21 |

[a]The irradiation time at which full eradication of the bacteria was achieved is provided in parentheses where relevant.

In the context of the studies against *S. aureus*, **PentaP** exhibited a $Log_{10}$ reduction value of 2.22, while **PentaBChl** had a higher value of 3.49. Typically, a $Log_{10}$ reduction value > 3 is required for a dye to be considered an effective antibacterial agent by the United States Food and Drug Administration.[35] Typical images from the bacterial colony counting process are provided in Figure 5. In studies against *E. coli*, **PentaP** exhibited a $Log_{10}$ reduction value of 6.39, corresponding to complete eradication, while **PentaBChl** had a $Log_{10}$ reduction value of 5.89. This is unusual in the context of Gram-(−) bacteria in the absence of the introduction of positively charged moieties, that can readily penetrate the lipopolysaccharide outer membrane. Similar data have been reported for synthetic tetraaryl-chlorins against Gram-(−) bacteria in recent years by Mack and coworkers, when the *meso*-phenyl rings are replaced with *meso*-thienyls or substituted with methoxy, hydroxy and/or methylthio groups.[15,36-39] The exact mechanism responsible for the high antimicrobial activity observed in these contexts with neutral PS dyes is not clear at this point but other examples have been reported previously by other research groups with porphyrins and chlorins containing *meso*-hydroxyphenyl and

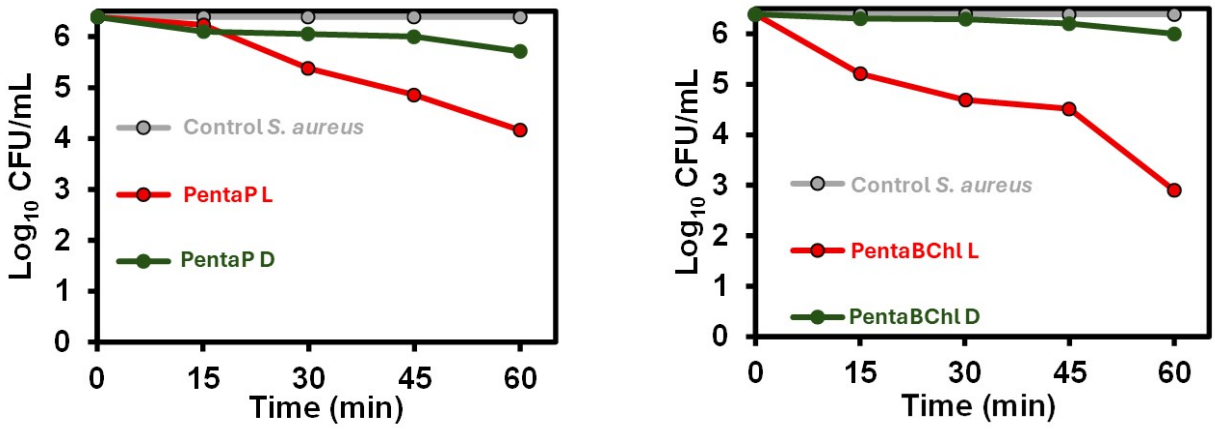


**Figure 3**. $Log_{10}$ reduction values against *S. aureus*. D and L refer to dark and light studies, respectively.

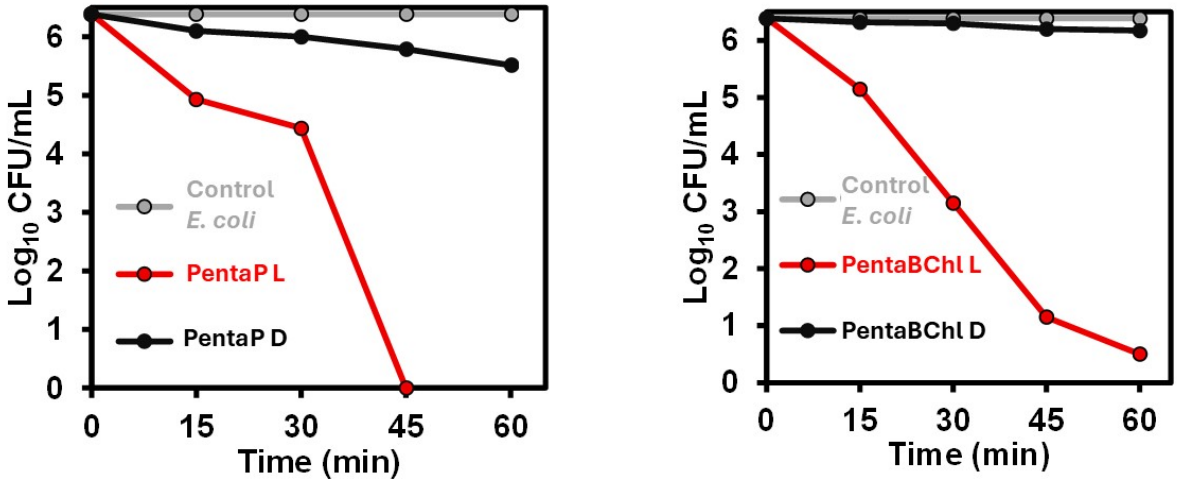


**Figure 4**. $Log_{10}$ reduction values for porphyrinoids against *E. coli*. D and L refer to the dark and light studies, respectively.

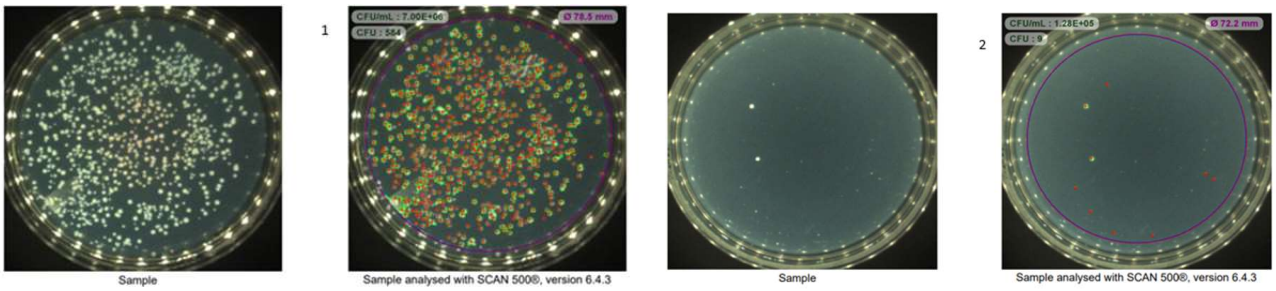


**Figure 5.** Images of *S. aureus* analyzed before (LEFT) and after (RIGHT) 45 min of photoirradiation with LED light.

*meso*-nitrophenyl rings[40-43] and curcumin I, which contains two 4-hydroxy-3-methoxyphenyl rings.[44] It is also noteworthy that Hohlfeld *et al*. reported high $Log_{10}$ reduction against Gram-(−) *P. aeruginosa* during PACT studies with 1,3,5,7-tetramethyl-2,6-diromoBODIPY core dyes with *meso*-pentafluorophenyl rings modified with thio-carbohydrates at the *para*-position.[45] It can perhaps be speculated that the aryl rings that were involved in these studies enhanced the lipo-philicity of the neutral PS dyes in the outer membrane of the Gram-(−) bacteria.[46]

### *Anticancer studies*

Figure 6 depicts the *in vitro* PDT activity studies against MCF-7 breast cancer cells used to calculate $IC_{50}$ values (Table 4) over the 0−100 μM concentration range under unexcited (dark) and excited (light) photodynamic conditions. At 0 μM, during both the dark toxicity and PDT activity studies no significant cell death was observed for cells treated with 5% DMSO in PBS. Neither of the dyes exhibits significant dark toxicity (Table 4). A relatively

low $IC_{50}$ value of 7.6 μM was observed for **PentaBChl** during the PDT activity studies, while 50% cell viability was not achieved with **PentaP**. **PentaBChl** hence exhibited a phototoxicity index (PI) value >13.2, based on the ratio of the $IC_{50}$ values obtained during the light and dark studies. Despite the significantly lower singlet oxygen quantum of 0.21, the $IC_{50}$ value was comparable to those reported previously by Mack and coworkers for tetraarylchlorins using directly comparable procedures (Table 4).[15,36-39] Fluorescence microscopy (Figure 7) was used to examine the morphologies of the MCF-7 breast cancer cells before and after photoirradiation.

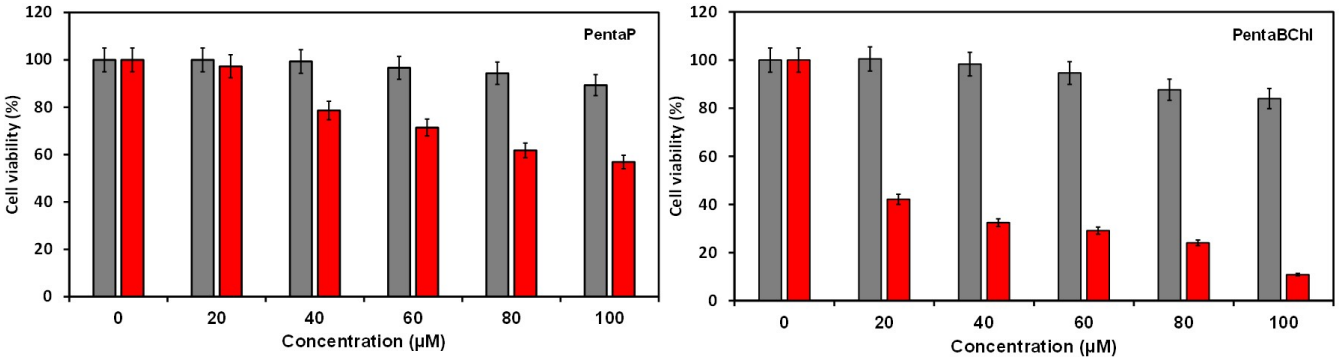


**Figure 6**. Cell viability values for **PentaP** and **PentaBChl** in the dark toxicity studies (gray bars) and after illumination with Thorlabs M595L3 and M730L4 LEDs (red bars), respectively. Error bars represent mean ± standard deviation.

**Table 4.** $IC_{50}$ values of **PentaBChl** and various free base tetraarylchlorins against MCF-7 cells with and without photoirradiation.

| Dye or *meso*-group | $\Phi_\Delta$ | $IC_{50}$ (μM) | | PI | Thorlabs LED | Time (min) | Dose ($J/cm^2$) | Ref. |
|---|---|---|---|---|---|---|---|---|
| | | Light | Dark | $IC_{50}$ (Light/Dark) | LED, Max. Output λ | | | |
| Tetraarylbacteriochlorin | | | | | | | | |
| **PentaBChl** | 0.21 | 7.6 | > 100 | > 13.2 | M730L4, 730 nm | 30 | 1.7 | -- |
| Tetraarylchlorins | | | | | | | | |
| Thien-2-yl | 0.60 | 3.5 | > 25 | > 7.1 | M660L4, 660 nm | 15 | 1.5 | [36] |
| 5-Bromothien-2-yl | 0.64 | 2.7 | > 25 | > 9.3 | M660L4, 660 nm | 15 | 1.5 | [36] |
| Phenyl | 0.55 | 15.8 | > 25 | > 1.6 | M660L4, 660 nm | 15 | 1.5 | [36] |
| Thiomethylphenyl | 0.40 | 7.8 | > 50 | > 6.4 | M660L4, 660 nm | 30 | 3.0 | [37] |
| 3-Methoxyphenyl | 0.59 | 22.4 | > 25 | > 1.1 | M625L3, 625 nm | 20 | 1.8 | [38] |
| | | 13.9 | | > 1.8 | M660L4, 660 nm | | 2.0 | |
| 4-Hydroxyphenyl | 0.58 | 15.5 | > 25 | > 1.6 | M625L3, 625 nm | 20 | 1.8 | [38] |
| | | 9.4 | | > 2.7 | M660L4, 660 nm | | 2.0 | |
| Vanillinyl | 0.62 | 10.8 | > 25 | > 2.3 | M625L3, 625 nm | 20 | 1.8 | [38] |
| | | 6.1 | | > 4.1 | M660L4, 660 nm | | 2.0 | |
| 4-Methoxyphenyl | 0.61 | 12.4 | > 25 | > 2.0 | M625L3, 625 nm | 20 | 1.8 | [39] |
| | | 13.9 | | > 1.8 | M660L4, 660 nm | | 2.0 | |

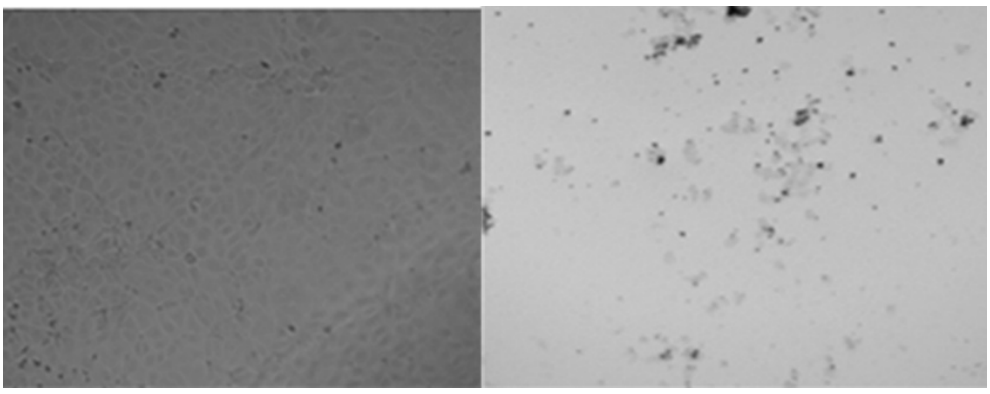

**Figure 7**: Morphologies of MCF-7 control cells at 0 μM (LEFT) and MCF cells after incubation with 100 μM **PentaBChl** and photoirradiation for 30 min with a Thorlabs M730L4 LED (RIGHT).

## Conclusions

During the PDT activity studies, a significantly lower $IC_{50}$ value of 7.6 μM was obtained against MCF-7 breast cancer cells for **PentaBChl** relative to the parent porphyrin **PentaP** dye, which retained cell viabilities > 50 μM. The $IC_{50}$ value was comparable to those reported previously by Mack and coworkers for tetraarylchlorins using directly comparable procedures,[15,36-39] despite the significantly lower $\Phi_\Delta$ value of 0.21 observed in DMSO. It was particularly noteworthy that high $Log_{10}$ reduction values were obtained for **PentaP** and **PentaBChl** against Gram-(−) *E. coli* during the PACT activity studies, even in the absence of positively charged moieties, in a manner similar to what has been observed recently by Mack and coworkers for tetraarylchlorins with *meso*-thienyl and *meso*-methylthiophenyl rings.[15,36-39] and had been reported previously against Gram-(−) *P. aeruginosa* by Hohlfeld *et al.* for 1,3,5,7-tetramethyl-2,6-diromoBODIPY core dyes with *meso*-pentafluorophenyl rings that are modified with thiocarbohydrates at the *para*-position.[45] Further PACT studies are in progress with chlorins and BChls prepared with a wider range of *meso*-aryl substituents to try to identify structure-property relationships in this context

**Acknowledgements**. Financial support was provided by the National Research Foundation (NRF) of South Africa through a SA-Flanders collaborative grant to JM, the DST/NRF Research Chairs Initiative−Professor of Medicinal Chemistry and Nanotechnology (uid: 62620), along with the Department of Science and Technology (DST) of South Africa to TN, and through PhD bursary scholarships to KGT and MML. Research reported in this publication was supported by the South African Medical Research Council with funds received from the South African National Department of Health and the UKRI Medical Research Council, with funds received from the UK Government's International Science Partnerships Fund. Theoretical calculations were carried out at the Centre for High Performance Computing in Cape Town. The Laser Rental Pool Programme of South Africa's National Photonics Centre facilitated several of the photophysicochemical measurements. This work was also supported by the Council for Scientific and Industrial Research (CSIR) of South Africa National Laser Centre through a CSIR African Laser Centre grant to JM, and by a Pearson-Young Memorial Trust MSc bursary to KGT.

**Author Contributions.** Kaisano Tauyakhale: conceptualization; methodology; formal analysis; validation; investigation; writing – original draft; visualization. Mahlatse Ledwaba: investigation; writing – review & editing. Earl Prinsloo: resources; methodology. John Mack: conceptualization; methodology; writing – review & editing; project administration; supervision; funding acquisition; visualization. Tebello Nyokong: resources; writing – review & editing; supervision.

## References

1. World Health Organization WHO. (2025, February 3). Cancer. Retrieved 05-12-2025 from *https://www.who.int/news-room/fact-sheets/detail/cancer*.
2. World Health Organization WHO. (2019, July 12). Cancer. Retrieved 05-12-2025 from *https://www.who.int/multimedia/details/globally1outof6deathsisduetocancer*.
3. Zhong L., Li Y., Xiong L., Wang W., Wu M., Yuan T., Yang W., Tian C., Miao Z., Wang T., Yang S. *Signal Transduct. Target. Ther.* **2021**, *6*, 201. DOI: 10.1038/s41392-021-00572-w.
4. Papac R.J. *Yale J. Biol. Med.* **2021**, 74, 391.
5. Hong W.K., Bromer R.H., Amato D.A., Shapshay S., Vincent M., Vaughan C., Willett B., Katz A., Welch J., Fofonoff S., Strong M.S. *Cancer* **1985**, 56, 1242–1245. DOI: 10.1002/1097-0142(19850915)56:6<1242::AID-CNCR2820560603>3.0.CO;2-Z.
6. Dougherty T.J., Gomer C.J., Henderson B.W., Jori G., Kessel D., Korbelik M., Moan J.E., Peng Q. *J. Natl. Cancer Inst.* **1998**, *90*, 889−905. DOI: 10.1093/jnci/90.12.889.
7. Zhang Q., He J., Wang Y., Yan-Chun L., Liu Z., Zhou B.N., Liu Y. *RSC Med. Chem.* **2020**, *11*, 427–437. DOI: 10.1039/c9md00558g.
8. Rajora M.A., Lou J.W.H., Zheng G. *Chem. Soc. Rev.* **2017**, *46*, 6433–6469. DOI: 10.1039/c7cs00525.
9. *Nanostructures for Antimicrobial Therapy* (Ficai A., Grumezescu A.M., Eds.), Elsevier: Amsterdam, Netherlands, **2017**. *https://www.sciencedirect.com/book/9780323461528/nanostructures-for-antimicrobial-therapy.*
10. Kumar G., Pant G., Hossain K., Ahmad A., Alshammari M.B. *ACS Omega* **2023**, *8*, 13492–13508. DOI: 10.1021/acsomega.3c00110.
11. Pucelik B., Sułek A., Drozd A., Stochel G., Pereira M.M., Pinto S.M.A., Arnaut L.G., Dąbrowski J.M. *Int. J. Mol. Sci.* **2020**, *21*, 2786. DOI: 10.3390/ijms21082786.
12. Pratavieira S., Uliana M.P., dos Santos Lopes N. S., Donatoni M.C., Linares D.R., de Freitas Anibal F., de Oliveira K.T., Kurachi C., de Souza C.W.O. *Photodiagn. Photodyn Ther.* **2021**, *34*, 102251. DOI: 10.1016/j.pdpdt.2021.102251
13. Costa-Tuna A., Chaves O.A., Loureiro R.J., Pinto S., Pina J., Serpa C. *Int. J. Biol. Macromol.* **2024**, *255*, 128210. DOI: 10.1016/j.ijbiomac.2023.128210.
14. Ethirajan, M., Chen, Y., Joshi, P., Pandey, R.K. *Chem. Soc. Rev.* **2011**, *40*, 340–362. DOI: 10.1039/b915149b.
15. Babu B., Mack J., Nyokong T. *Dalton Trans.* **2023**, 52, 5000–5018. DOI: 10.1039/d3dt00603d.
16. Majumdar P., Raju N., Zhao J. *J. Mater. Chem. C* **2014**, *2*, 5982–5997. DOI: 10.1039/c4tc00659c.
17. Li, D., Liu, P., Tan, Y., Zhang, Z., Kang, M., Wang, D., Tang, B. Z. *Biosensors* **2022**, *12*, 722. DOI: 10.3390/bios12090722.
18. Wu M., Liu Z., Zhang W. *Chem. Sci.* **2021**, *12*, 1295–1301. DOI: 10.1039/d0sc05525e.
19. Goslinski T., Piskorz J. *J. Photochem. Photobiol. C* **2011**, *12*, 304–321. DOI: 10.1016/j.jphotochemrev.2011.09.005
20. Frank H., Cogdell R. *Compr. Biophys.* **2012**, *8*, 94–114. DOI: 10.1016/b978-0-12-374920-8.00808-0.
21. Hamblin M.R., Hasan, T. *Photochem. Photobiol. Sci.* **2004**, *3*, 436–450. DOI: 10.1039/b311900a.
22. Rodrigues A.d.C., Bilha J.K., Pereira P.R.M., de Souza C.W.O., Passarini M.R.Z., Uliana M.P. *Braz. J. Microbiol.* **2024**, *55*, 1139–1150. DOI: 10.1007/s42770-024-01278-1
23. Demas J.N., Crosby G.A. *J. Phys. Chem.* **1971**, *75*, 991–1024. DOI: 10.1021/j100677a001.
24. Tran Thi T.H., Desforge C., Thiec C., Gaspard S. *J. Phys. Chem.* **1989**, *93*, 1226–1233. DOI: 10.1021/j100341a013.

25. Redmond R.W., Gamlin J.N. *Photochem. Photobiol.* **1999**, *70*, 391−475. DOI: 10.1111/j.1751-1097.1999.tb08240.x.
26. Adler A.D., Longo F.R., Finarelli, J.D., Goldmacher J., Assour J., Korsakoff L. *J. Org. Chem.* **1967**, *32*, 476. DOI: 10.1021/jo01288a053.
27. Mosmann, T. *J. Immunol. Methods* **1983**, *65*, 55–63. DOI: 10.1016/0022-1759(83)90303-4.
28. Frisch M.J., Trucks G.W., Schlegel H.B., Scuseria G.E., Robb M.A., Cheeseman J.R., Scalmani G., Barone V., Mennucci B., Petersson G.A., Nakatsuji H., Caricato M., Li X., Hratchian H.P., Izmaylov A.F., Bloino, J., Zheng, G., Sonnenberg J.L., Hada M., Ehara M., Toyota K., Fukuda R., Hasegawa J., Ishida M., Nakajima T., Honda Y., Kitao O., Nakai H., Vreven T., Montgomery J.A. Jr, Peralta J.E., Ogliaro F., Bearpark M., Heyd J.J., Brothers E., Kudin K.N., Staroverov V.N., Kobayashi R., Normand J., Raghavachari K., Rendell A., Burant J.C., Iyengar S.S., Tomasi J., Cossi M., Rega N., Millam J.M., Klene M., Knox J.E., Cross J.B., Bakken V., Adamo C., Jaramillo J., Gomperts R., Stratmann R.E., Yazyev O., Austin A.J., Cammi R., Pomelli C., Ochterski J.W., Martin R.L., Morokuma K., Zakrzewski V.G., Voth G.A., Salvador P., Dannenberg J.J., Dapprich S., Daniels A.D., Farkas Ö., Foresman J.B., Ortiz J.V., Cioslowski J., Fox D.J. Gaussian 09, Revision E.01, Gaussian Inc., Wallingford CT, **2009**.
29. Yanai T., Tew D.P., Handy, N.C. *Chem. Phys. Lett.* **2004**, *393*, 51–57. DOI: 10.1016/j.cplett.2004.06.011.
30. Huang Y.Y., Mroz P., Zhiyentayev T., Sharma S.K., Balasubramanian T., Ruzie C., Krayer M., Fan D., Borbas K.E., Yang E., Kee H.L., Kirmaier C., Diers J.R., Bocian D.F., Holten D., Lindsey J.S., Hamblin, M.R. *J. Med. Chem.* **2010**, *53*, 4018–4027 DOI: 10.1021/jm901908s.
31. Zhu W., Gao Y.H., Liao P.Y., Chen D.Y., Sun N.N., Nguyen Thi P.A., Yan Y.J., Wu X.F., Chen, Z.L. *Eur. J. Med. Chem.* **2018**, *160*, 146–156 DOI: 10.1016/j.ejmech.2018.10.005.
32. Gouterman M., Wagnière GH, Snyder, L.C. *J. Mol. Spectrosc.* **1963**, *11*, 108–127. DOI: 10.1016/0022-2852(63)90011-0.
33. Michl J. *Tetrahedron* **1984**, *40*, 3845–3934. DOI: 10.1016/S00 40-4020(01)99999-5.
34. Mack J. *Chem. Rev.* **2017**, *117*, 3444–3478. DOI: 10.1021/acs.chemrev.6b00568.
35. Seal L.A., Rizer R.L., Maas-Irslinger R. *Am. J. Infect. Control* **2005**, *33*, 207–216. DOI: 10.1016/j.ajic.2004.11.009.
36. Babu B., Sindelo A., Mack J., Nyokong, T. *Dyes Pigm.* **2021**, *185*, 108886. DOI: 10.1016/j.dyepig.2020.108886.
37. Dingiswayo S., Burgess K., Babu B., Mack J., Nyokong T. *ChemPlusChem* **2022**, *87*, e202200115. DOI: 10.1002/cplu.202200115.
38. Soy R.C., Babu B., Mack J., Nyokong T. *Molecules* **2023**, *28*, 4030. DOI: 10.3390/molecules28104030.
39. Soy R.C., Babu B., Mack J., Nyokong T. *Photodiagn. Photodyn. Ther.* **2023**, *44*, 103815. DOI: 10.1016/j.pdpdt.2023.103815.
40. Maldonado-Carmon N., Ouk T.-S., Leroy-Lhez S. *Photochem. Photobiol. Sci.* **2022**, *21*, 113–145. DOI: 10.1007/s43630-021-00128-5.
41. Wikene K.O., Bruzell E., Tønnesen, H.H. *J. Photochem. Photobiol. B* **2015**, *148*, 188–196. DOI: 10.1016/j.jphotobiol.2015.04.022.
42. Bair K.L., Shafirstein G., Campagnari, A.A. *Front. Microbiol.* **2020**, *11*, 1–9. DOI: 10.3389/fmicb.2020.558482.
43. Rahimi R., Fayyaza F., Rassab M., Rabbania, M. *Iran. Chem. Commum.* **2015**, *4*, 175–185.
44. Law S.K., Leung A.W.N., Xu C. *Pharm.* **2023**, *17*, 34. DOI: 10.3390/ph17010034.
45. Hohlfeld B.F., Gitter B., Flanagan K.J., Kingsbury C.J., Kulak N., Senge M.O., Wiehe A. *Org. Biomol. Chem.* **2020**, *18*, 2416–2431. DOI: 10.1039/d0ob00188k .
46. El-Saadony M.T., Saad A.M., Mohammed D.M., Alkafaas S.S., Ghosh S., Negm S.H., Salem H.M., Fahmy M.A., Mosa W.F.A., Ibrahim E.H., AbuQamar S.F., El-Tarabily K.A. *Front. Immunol.* **2025**, *16*, 1603018. DOI: 10.3389/fimmu.2025.1603018.


*Received 18.12.2025*
*Accepted 02.03.2026*